


# The Trajectory of the ( $\eta^5$ -Cyclopentadienyl)cobalt-Mediated Cycloisomerization of Ene-Yne-Ene-Type Allyl Propargylic Ethers to Furans: A DFT Appraisal

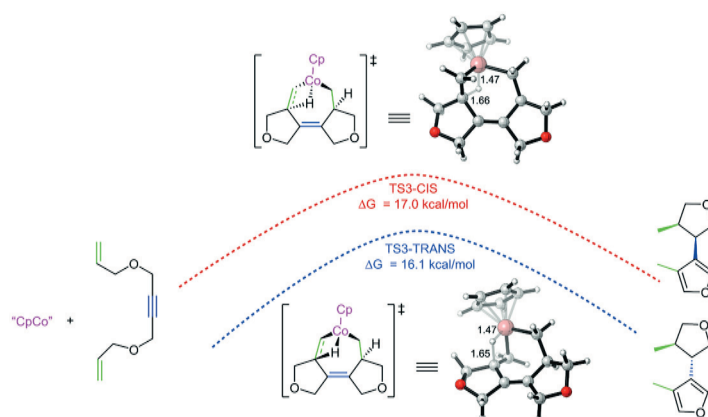
Jonathan J. Wong<sup>a</sup>Xiangyang Chen<sup>a</sup>Kendall N. Houk<sup>\*a</sup> K. Peter C. Vollhardt<sup>\*b</sup> 

<sup>a</sup> Department of Chemistry and Biochemistry, University of California, Los Angeles, Los Angeles, California 90095, USA  
houk@chem.ucla.edu

<sup>b</sup> Department of Chemistry, University of California at Berkeley, Berkeley, California 94720-1460, USA  
kpcv@berkeley.edu

Congratulations to Professor Sarah Reisman at the California Institute of Technology for having been chosen as the first recipient of the Dr. Margaret Faul Award for Women in Chemistry

Published as part of the  
Special Issue dedicated to Prof. Sarah Reisman, recipient of the 2019 Dr. Margaret Faul Women in Chemistry Award



Received: 10.08.2021

Accepted after revision: 15.09.2021

Published online: 15.09.2021

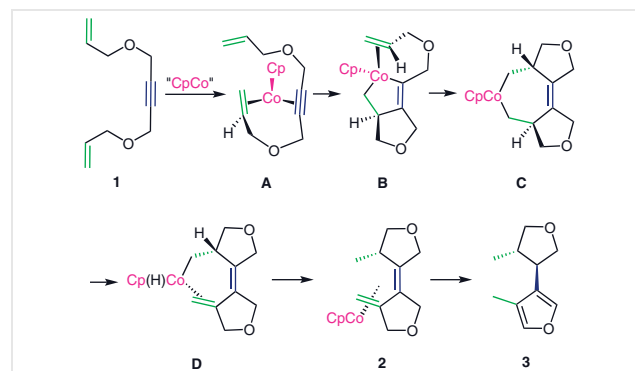
DOI: 10.1055/a-1645-2632; Art ID: ss-2021-m0475-st

**Abstract** The mechanisms by which the complexes  $\text{CpCoL}_2$  ( $\text{Cp} = \text{C}_5\text{H}_5$ ;  $\text{L} = \text{CO}$  or  $\text{CH}_2=\text{CH}_2$ ) mediate the cycloisomerizations of  $\alpha,\delta,\omega$ -enynenes containing allylic ether linkages are probed by DFT methods. The outcomes corroborate experimental results and provide energetic and structural details of the trajectories leading to 3-(oxacyclopentyl or cycloalkyl)furans via the intermediacy of isolable  $\text{CpCo-}\eta^4$ -dienes. They comprise initial stereoselective complexation of one of the double bonds and the triple bond, rate-determining oxidative coupling to a triplet 16e cobalta-2-cyclopentene, and terminal double bond docking, followed by stereocontrolled insertion to assemble intermediate *cis*- and *trans*-fused triplet cobalta-4-cycloheptenes. A common indicator of the energetic facility of the latter is the extent of parallel alignment of the alkene moiety and its target  $\text{Co-C}\alpha$  bond. The cobalta-4-cycloheptenes transform further by  $\beta$ -hydride elimination–reductive elimination to furnish  $\text{CpCo-}\eta^4$ -dienes, which are sufficiently kinetically protected to allow for their experimental observation. The cascade continues through cobalt-mediated hydride shifts and dissociation of the aromatic furan ring. The findings *in silico* with respect to the stereo-, regio-, and chemoselectivity are in consonance with those obtained *in vitro*.

**Key words** DFT, enynes,  $\beta$ -hydride elimination, cobalt, cycloisomerization, furans

We recently reported on the cycloisomerizations of  $\alpha,\delta,\omega$ -enynenes containing allylic ether linkages mediated catalytically and stoichiometrically by  $\text{CpCoL}_2$  ( $\text{Cp} = \text{C}_5\text{H}_5$ ;  $\text{L} = \text{CO}$  or  $\text{CH}_2=\text{CH}_2$ ) to furnish 3-(oxacyclopentyl or cycloalkyl)furans via the intermediacy of isolable  $\text{CpCo-}\eta^4$ -dienes.<sup>1</sup> In the simplest case, substrate **1** was seen to convert into

*trans* isomer **3** with catalytic  $\text{CpCo}(\text{CO})_2$  in boiling and irradiated PhMe in 70% yield, while intermediate **2** could be intercepted when **1** was exposed to one equivalent of  $\text{CpCo}(\text{CH}_2=\text{CH}_2)$  at 0 °C, also in 70% yield. In both cases, inspection of the crude reaction mixtures by <sup>1</sup>H NMR revealed the presence of 2–3% of the corresponding stereoisomers. A very tentative mechanism was formulated based on related art<sup>2,3</sup> and geared toward reproducing the *syn* (methyl to  $\text{Cp-Co}$ ) stereochemistry in **2** and the *trans* constitution of **3** (Scheme 1). Accordingly, it featured the *syn* (with respect to the ether bridge) disposed enyne complex **A**, an arbitrary choice, since the subsequent oxidative coupling to the cobaltacyclopentene (not formulated) is stereoconvergent, followed by intermediate **B**, which sets the eventual stereochemistry in **2** and **3**. Insertion of the appended double bond results in the *trans* compound **C**, from which  $\beta$ -hydride



**Scheme 1** Mechanism of the cycloisomerization of **1** into **3**

elimination engenders **D**. Reductive elimination to liberate the methyl group then assembles **2**, and subsequent hydride shifts provide the final furan **3**.

While Scheme 1 provides a plausible mechanistic blueprint of the reaction, its details raise a number of questions. Thus, what are the relative energies of the proposed species? What are the barriers associated with their interconversion? What is the feasibility of alternative structures? Moreover, investigations of the scope and limitations of this process showed much less related stereoselectivity, in addition to uncovering some notable instances of chemo-, regio-, and more complex diastereoselectivity. This paper aims to provide answers to these queries by a DFT computational scrutiny of the basic conversion of **1** into **3**, as well as that of variants of **1** that were investigated in our experimental work.<sup>1</sup> The intramolecular cyclization of dienyne has not been the subject of computational analysis, and we hope that our results will provide an increased understanding of related experimental investigations.<sup>3</sup> In addition, some of the computed individual steps bear some similarity to calculated transformations in the literature, providing a corresponding complement.<sup>4,5</sup> The present estimates were obtained at the PW6B95-D3BJ/def2-TZVP, SMD(PhMe)//B3LYP-D3/6-31G(d)-SDD(Co) level of theory. Coordinatively unsaturated CpCo complexes were triplets, all energetically favored over their corresponding singlet states (see the Supporting Information). Energies are reported in kcal mol<sup>-1</sup> and distances in Ångströms. For a continuous energy diagram of Figures 1, 4, 6, and 8, and xyz tabulations, see the Supporting Information.

Our estimates start with **1** and CpCo(CO)<sub>2</sub> (−20.6 kcal mol<sup>-1</sup>), which, upon irradiation, leads to decarbonylation to form a reactant enyne complex **RC-SYN-H**. It features the *syn* disposition of the alkenyl hydrogen to the metal and is assigned a Δ*G* value of 0.0 kcal mol<sup>-1</sup> (Figure 1). The corresponding diastereomer **RC-ANTI-H** (not shown) is less stable by 15.7 kcal mol<sup>-1</sup>. While such isomers are typically close in energy,<sup>5,6</sup> here the constraints of the ether bridge in the *anti* form obviate the favorable near parallel orientation of the unsaturated fragments of the enyne ligand present in the *syn* configuration. **RC-SYN-H** progresses via oxidative coupling to a 16-electron triplet intermediate **IN1-T**, more stable than **RC-SYN-H** by 11.3 kcal mol<sup>-1</sup> and with a free energy barrier of 18.9 kcal mol<sup>-1</sup> (**TS1**).

From **IN1-T**, coordination of the appended alkene can engender four possible singlet stereoisomers **IN1** in the various combinations of *cis*, *trans*, *exo*, and *endo* (Figure 2). Here, *cis* denotes that subsequent ligated double bond insertion would lead to triplet *cis*-metallacycloheptene **IN2-T-CIS** with the tertiary hydrogen atoms positioned *cis* to each other, while *trans* corresponds to the complex preceding **IN2-T-TRANS**. Similarly, *endo* and *exo* refer to the orientation of the ether linker between the complexed ene moiety and the carbon backbone of the metallacycle, as in Diels–Alder terminology. As shown in Figure 2, among the isomers of **IN1**, the **TRANS-EXO** configuration is the most stable, followed by **CIS-ENDO** (+0.1 kcal mol<sup>-1</sup>), **CIS-EXO** (+5.3 kcal mol<sup>-1</sup>), and **TRANS-ENDO** (+8.2 kcal mol<sup>-1</sup>). The origins of the increasing destabilization along the series are difficult to pinpoint and appear to be composed of incremental con-

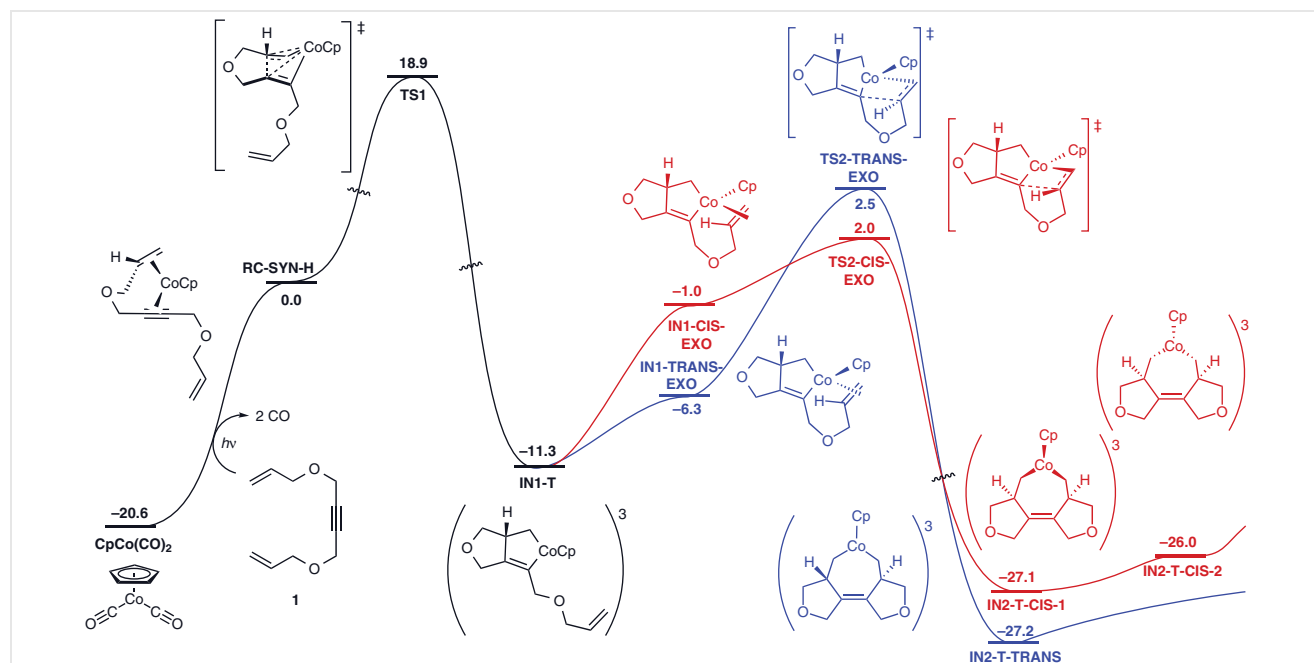


**Figure 1** Computed Δ*G* profile of the reaction of **1** with CpCo(CO)<sub>2</sub> to give the cobaltacycloheptene intermediate **IN2** (**C** in Scheme 1)

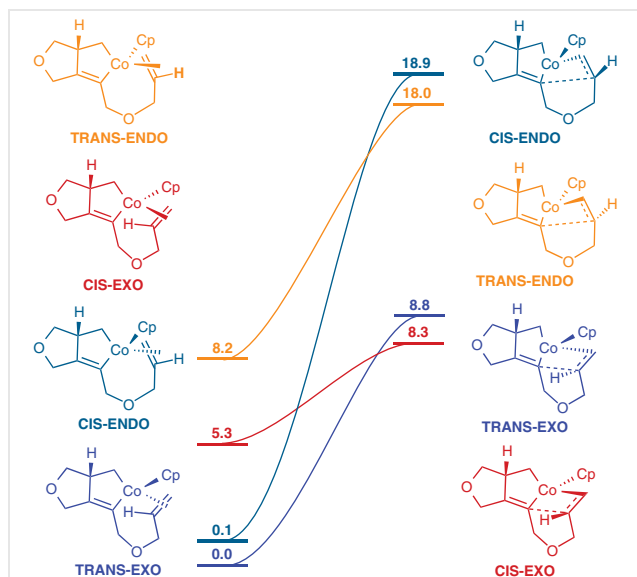


**Figure 2**  $\Delta\Delta G$  values (kcal mol<sup>-1</sup>) associated with the insertion of the ligated double bond in the diastereomers of **IN1** via **TS2**

tributions of increasing eclipsing, bond angle, and transannular strain distributed over the entire framework, (see xyz data in the Supporting Information). Interestingly, on subsequent insertion of the ligated double bond into the Co–C linkage, substantial reorganization of the associated energy values occurs. The *endo* transition states are disfavored by ~10 kcal mol<sup>-1</sup> relative to their *exo* counterparts. Indeed, visually (see xyz data in the Supporting Information), the latter display pseudo-chair conformations of the forming hy-

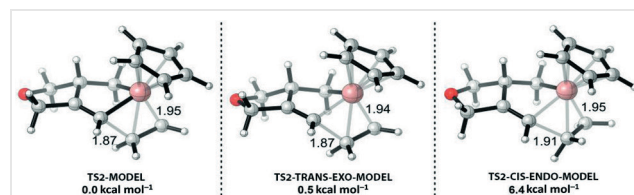


**Figure 3** Models for **TS2** featuring ethene

drofuran ring atoms and Co, whereas the former show highly distorted corresponding arrays. As a result, the *exo* structures exhibit a near parallel (optimal)<sup>5e,7</sup> geometry of the inserting alkene moiety and its target Co–C $\alpha$  bond, compared to their higher energy relatives (absolute dihedral angles Co–C $\alpha$ –CH–CH<sub>2</sub> in order of increasing energies: 5, 2, 39, and 29°, see the Supporting Information).

To probe the extent to which the *exo* insertion pathway is favored intrinsically, a model system featuring ethene was computed, generating the structure represented by **TS2-MODEL** (Figure 3), in which the double bond approaches from the opposite side of the tertiary hydrogen situated on the dihydrofuran moiety and is almost perfectly aligned with the neighboring Co–C $\alpha$  bond (dihedral angle 0.5°).

The alternative did not produce a stationary point along the potential energy surface. The structure and energy of **TS2-MODEL** was then compared with those of truncated **TS2-TRANS-EXO** and **TS2-CIS-ENDO**, in which the H<sub>2</sub>COCH<sub>2</sub> linker had been removed: **TS2-TRANS-EXO-MODEL** and **TS2-CIS-ENDO-MODEL** (Figure 3). It is evident in the transition state bond lengths and orientation of the incoming

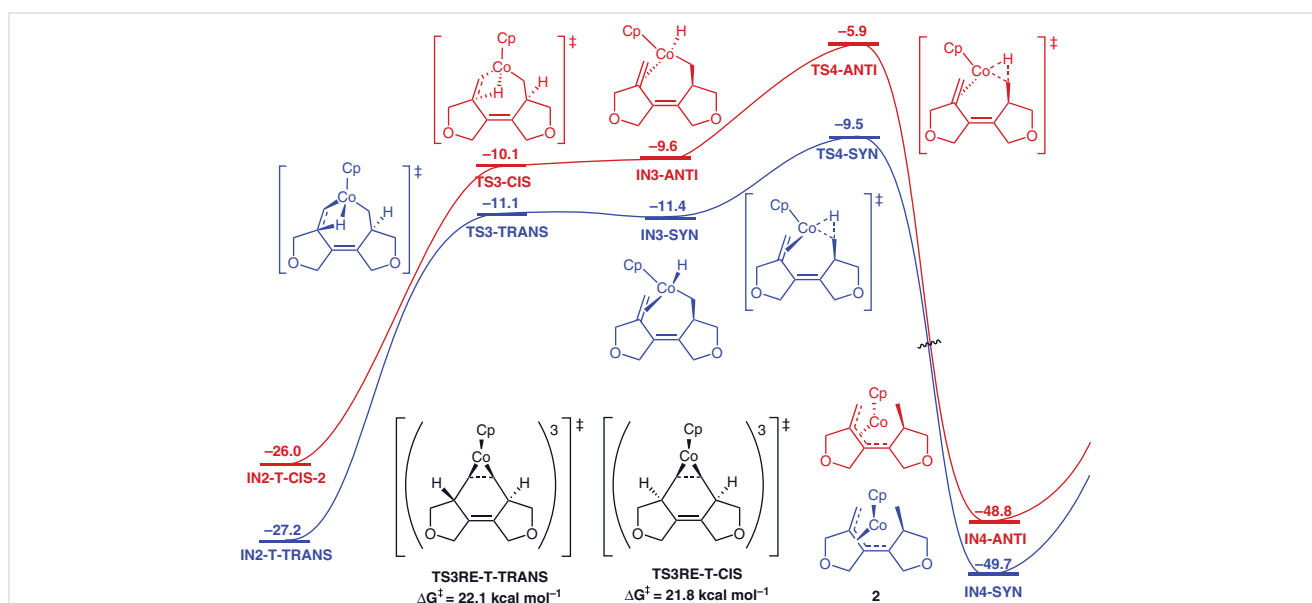


**Figure 4** Hydride transfer from **IN2** to render 1,3-butadiene complexes **IN4** (**IN4-SYN** = **2**)

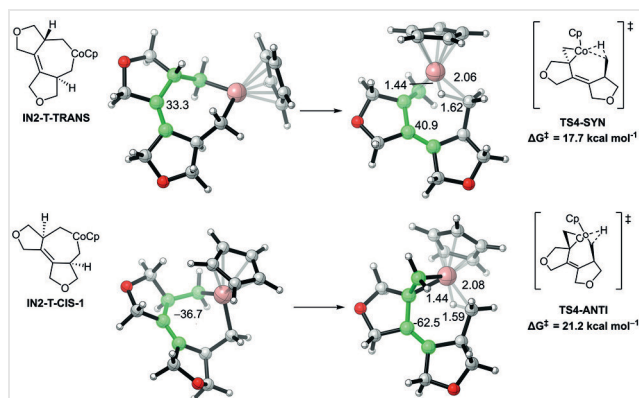


**Figure 5** Distortions of the green-highlighted dihedral angles *en route* from the two isomers of **IN-2** to the respective transition states **TS4**

ethene that the *trans-exo* conformation is most similar to **TS2-MODEL**, with a difference in electronic energy of only 0.5 kcal mol<sup>-1</sup>. Its *endo* counterpart enforces an unfavorable trajectory of the double bond to the tune of 6.4 kcal mol<sup>-1</sup>, accounting for most of the energy difference (10.1 kcal mol<sup>-1</sup>, Figure 2) between **TS2-TRANS-EXO** and **TS2-CIS-ENDO**. The additional increment of 3.7 kcal mol<sup>-1</sup> has its likely origin in torsional strain in the forming hydrofuran ring.<sup>5e,7</sup>

Accordingly, and returning to Figure 1, from **IN1-T** (−11.3 kcal mol<sup>-1</sup>), coordination of the double bond leads to either **IN1-CIS-EXO**, located 1.0 kcal mol<sup>-1</sup> below the starting point **RC-SYN-H**, or **IN1-TRANS-EXO**, for which the corresponding value is 6.3 kcal mol<sup>-1</sup>. From **IN1-TRANS-EXO**, we reach **TS2-TRANS-EXO** (2.5 kcal mol<sup>-1</sup>) with an activation barrier of 13.8 kcal mol<sup>-1</sup> to form **IN2-T-TRANS** (−27.2

kcal mol<sup>-1</sup>). Alternatively, from **IN1-CIS-EXO**, we get to **IN2-T-CIS-1** (−27.1 kcal mol<sup>-1</sup>) with a barrier of 13.3 kcal mol<sup>-1</sup> via **TS2-CIS-EXO** (2.0 kcal mol<sup>-1</sup>). One notes that the two lowest energy transition states **TS2** toward **IN-2** determine the product stereochemistry in **2** (blue pathway) and its *cis* relative (red pathway), as the associated exothermicities (29–30 kcal mol<sup>-1</sup>) are larger than the energies of all subsequent steps (*vide infra*). The computed TS energy difference is extremely small (0.5 kcal mol<sup>-1</sup>), actually slightly favoring the minor *cis* product *in silico*, an incongruence that may be ascribed to the inherent variability between computation and experiment. This difference inverts, but is even smaller in **IN2**, the *trans* isomer being more stable than its *cis* relative by only 0.1 kcal mol<sup>-1</sup>.

The stage is now set for the next step of the overall mechanism, namely β-hydride elimination. While irrelevant for **IN2-T-TRANS**, **IN2-T-CIS-1** must undergo an envelope flip<sup>8</sup> to access the hydrogen atoms on the opposite face to form **IN2-T-CIS-2** (−26.0 kcal mol<sup>-1</sup>), with the minor energetic cost of 1.1 kcal mol<sup>-1</sup> (Figure 1). The β-hydride eliminations take place through the trio of states **TS3**, **IN3**, and **TS4** to reach the very closely energetic **IN4-ANTI** (−48.8 kcal mol<sup>-1</sup>) and the experimentally isolated **IN4-SYN** (**2**) (−49.7 kcal mol<sup>-1</sup>), accompanied by a >40 kcal mol<sup>-1</sup> energetic drop from **TS4** (Figure 4). Here, *syn* denotes that the metal center is bound to the ene-π frame from the same side as the Co-methylene bridge (and eventual methyl group), while for *anti* it is on the opposite face. For both trios, the energies are very similar, the surfaces in this region are very flat, and the relative energies of different species vary depending upon whether *E*, *H*, or *G* are compared. Although there are ripples on the surface, the hydride transfer to form **IN4**

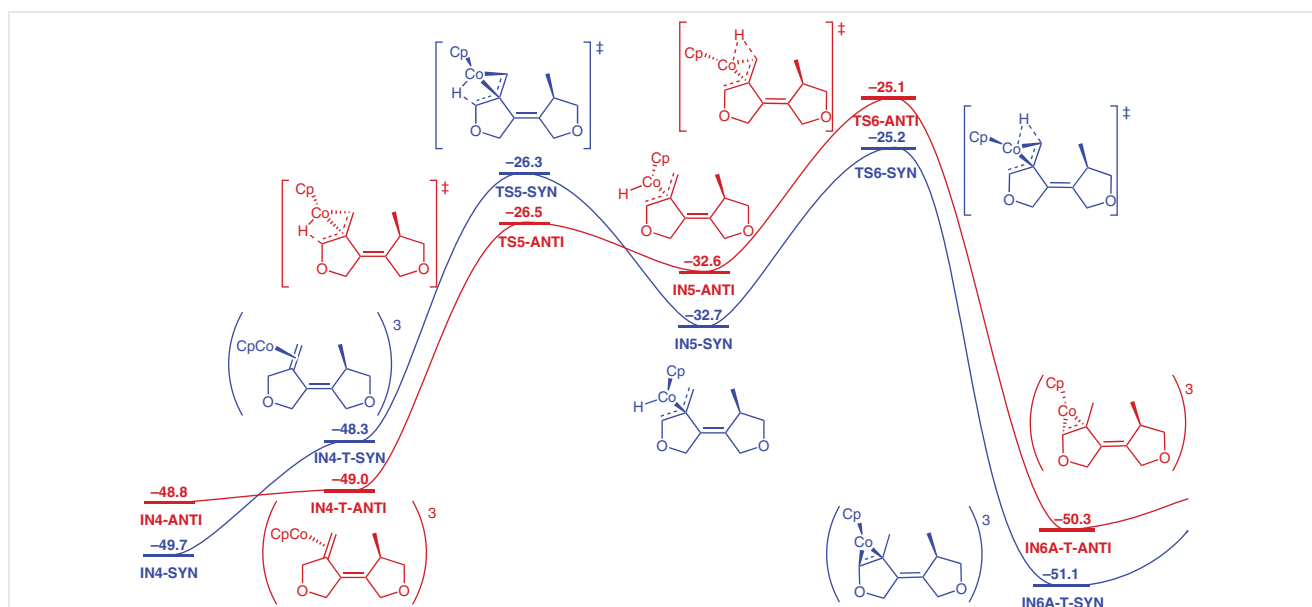
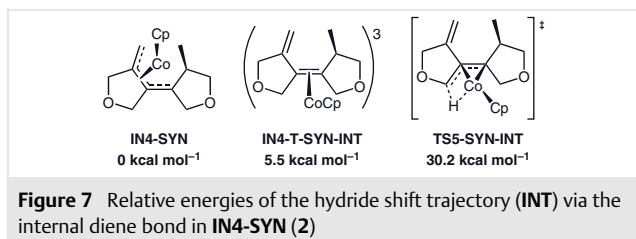


**Figure 6** First double bond shift from exocyclic **IN4** to endocyclic **IN6A-T** by hydrogen activation



occurs without a significant lifetime of the Co hydride intermediate. Not surprisingly, reductive elimination of cobaltacycloheptenes **IN2** en route to the corresponding fused cyclohexenes resulted in relatively higher triplet transition states **TS3RE-T-TRANS** and **TS3RE-T-CIS** (−5.1 and −4.2 kcal mol<sup>−1</sup>, for *trans* versus *cis*, respectively). Coordinative involvement of the facing double bond was geometrically thwarted.

The difference in transition state energies of 3.6 kcal mol<sup>−1</sup> between **TS4-SYN** and **TS4-ANTI**, in favor of the former and eventually ending in final furan **2**, is the largest along the entire reaction coordinate, warranting some speculation as to its origin. Indeed, inspection of the green-highlighted dihedral angles in Figure 5 indicates that reaching **TS4-ANTI** entails a much larger structural distortion (25.8°, starting from **IN2-CIS-1**) than the favored alternative (7.6°).

We are now ready for the evaluations of the series of hydride shifts that aromatize the 3,4-bisalkylidene ligand in **IN4**. As anticipated,<sup>2a,b,9</sup> these proceed via allylic transposi-

tions. To simplify the narrative, only the (blue) trail to the final isolated product **3** will be described, since it parallels closely that followed by the other isomer (red). It starts by an  $\eta^4$  to  $\eta^2$  change in coordination from **IN4-SYN** (−49.7 kcal mol<sup>−1</sup>) to the triplet terminal complex **IN4-T-SYN** (−48.3 kcal mol<sup>−1</sup>), slightly uphill by 1.4 kcal mol<sup>−1</sup> (Figure 6). The regiochemical alternative shift to the internal double bond (**IN4-T-SYN-INT**) is disadvantaged by an additional 5.5 kcal mol<sup>−1</sup> (Figure 7).

From **IN4-T-SYN**, a 1,3-hydride shift takes place via C–H activation through **TS5-SYN** (−26.3 kcal mol<sup>−1</sup>), with an energy barrier of 23.4 kcal mol<sup>−1</sup> from **IN4-SYN**. [The corresponding step from **IN4-T-SYN-INT** requires 30.2 kcal mol<sup>−1</sup> (**TS5-SYN-INT**, Figure 7)]. The result is the 18-electron allyl hydride complex **IN5-SYN** (−32.7 kcal mol<sup>−1</sup>). The rate-determining step for the double bond transposition is its reductive elimination via **TS6-SYN** (−25.2 kcal mol<sup>−1</sup>) with a hurdle of 24.5 kcal mol<sup>−1</sup> from **IN4-SYN** to yield the triplet intermediate **IN6A-T-SYN** (−51.1 kcal mol<sup>−1</sup>). This computed barrier is commensurate with the isolation of **2** when the isomerization of **1** is run at 0 °C and the further conversion of the former on heating. At this point (Figure 8), a haptotropic shift to **IN6B-T-SYN** (−50.8 kcal mol<sup>−1</sup>) is kinetically accessible with an energetic expenditure of only 8.3 kcal mol<sup>−1</sup> via **TSIN6-T-SYN** (−42.8 kcal mol<sup>−1</sup>). Renewed allylic C–H activation requires 22.9 kcal mol<sup>−1</sup> to climb over **TS7-SYN** (−27.9 kcal mol<sup>−1</sup>), resulting in allyl hydride intermediate **IN7-SYN** (−39.2 kcal mol<sup>−1</sup>). The final reductive elimination proceeds through **TS8-SYN** (−31.1 kcal mol<sup>−1</sup>), 8.1 kcal mol<sup>−1</sup> uphill, to the triplet  $\eta^2$ -furan complex **IN8-T-SYN**

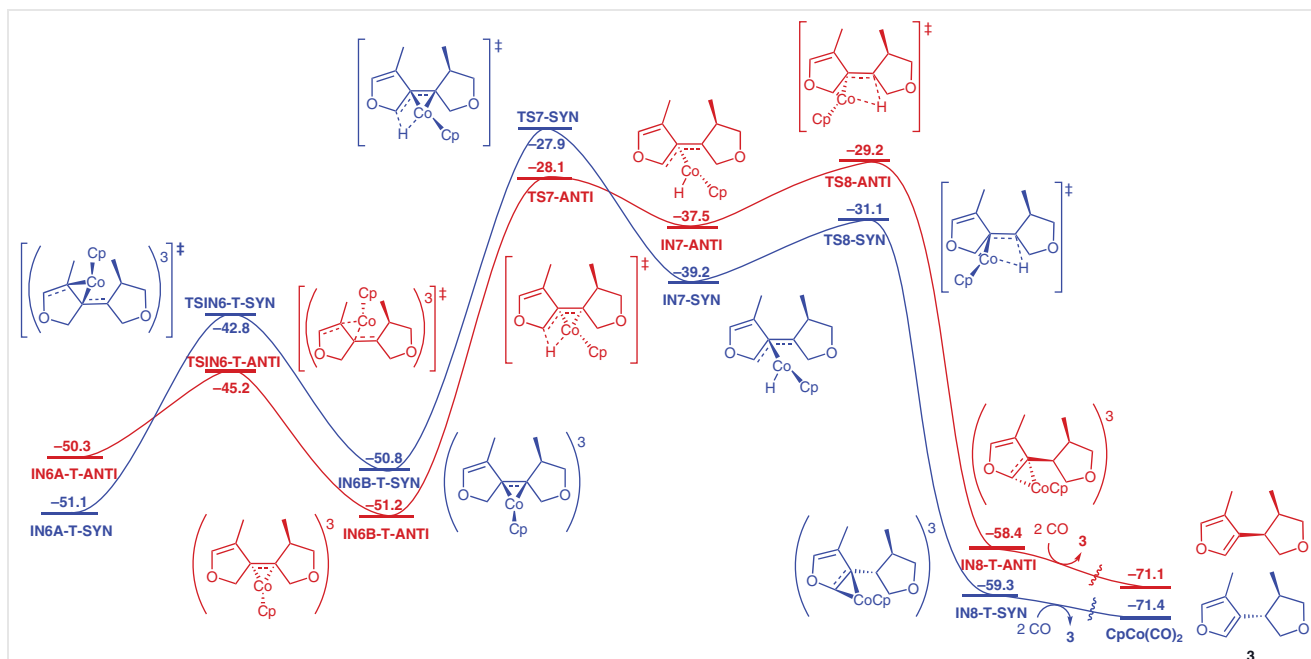


**Figure 8** A haptotropic shift and second hydride transfer from **IN6** to furnish eventually product **3**



( $-59.3 \text{ kcal mol}^{-1}$ ), with an energy gain of  $20.1 \text{ kcal mol}^{-1}$ . To estimate the exothermicity of the overall conversion of **1** into **3**, the regeneration of the catalyst with CO and extrusion of product was computed at  $-71.4 \text{ kcal mol}^{-1}$  relative to the reactant complex **RC-SYN-H**, providing a  $\Delta G_{1 \rightarrow 3}$  value of  $50.8 \text{ kcal mol}^{-1}$ . The corresponding *cis* isomer is only  $0.3 \text{ kcal mol}^{-1}$  less stable and its (red) path of formation from **IN4-ANTI** is energetically very close to that resulting in **3**.

Having established the qualitative and quantitative details of Scheme 1, computational attention turned to understanding the effects of structural variations in the order reported in the experimental account.<sup>1</sup> The first to be addressed concerned the failure of 1,4-bis[(3-methyl-2-butenyl)oxy]but-2-yne (**1-Me<sub>4</sub>**), in which **1** has been exhaustingly adorned with terminal additional methyl groups, to undergo cycloisomerization. Instead, two molecules of the starting material combine to couple the individual triple bonds and one of the appended double bonds to furnish the [2+2+2] cycloaddition product (Scheme 2). Molecular models indicate qualitatively the severe steric hindrance imposed by the methyl substituents on the initial stages of the process. Indeed, computationally, attempts to dock the external alkene unit to the CpCo in **IN1Me<sub>4</sub>-T** (Figure 9) did not locate a minimum, and further insertion via **TS2Me<sub>4</sub>-TRANS-EXO** and **TS2Me<sub>4</sub>-CIS-EXO**, respectively, resulted in considerably higher relative barriers ( $37.2$  and  $35.0 \text{ kcal mol}^{-1}$ ), when compared to those for **IN1** in Figure 2. Inspection of the calculated structures reveals several destabilizing non-bonded interactions ( $<2.4 \text{ \AA}$  separation) of the hydrogens of the methyl substituents with those of the remainder of the molecule.<sup>10</sup> For **TS2Me<sub>4</sub>-TRANS-EXO**, the closest such separation is  $1.80 \text{ \AA}$ , whilst for **TS2Me<sub>4</sub>-CIS-EXO**, it is  $1.92 \text{ \AA}$ . Accordingly, it appears that the intramolecular insertion of the hindered alkene unit is thwarted and the intermolecular implantation of the comparatively less hindered triple bond of a second molecule of substrate takes over.

Intriguingly, removing two of the methyl groups from **1-Me<sub>4</sub>**, as in **1-Me<sub>2</sub>** (Scheme 3), reinstated the cycloisomerization pathway, which proceeded with complete regio-

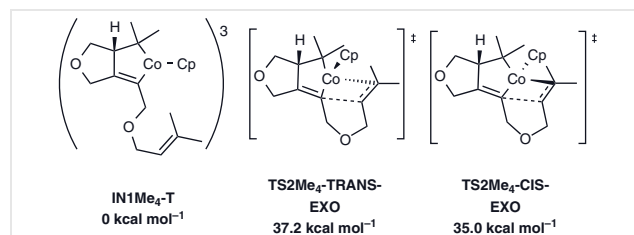
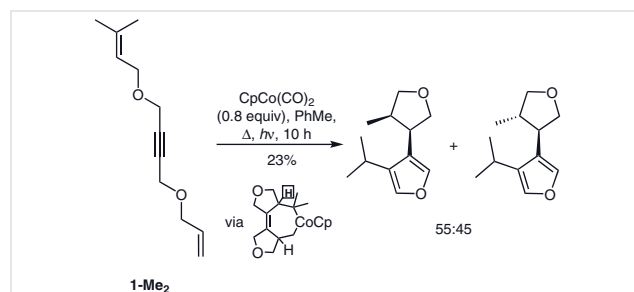


**Figure 9** Species derived from the interaction of CpCo with **1-Me<sub>4</sub>**

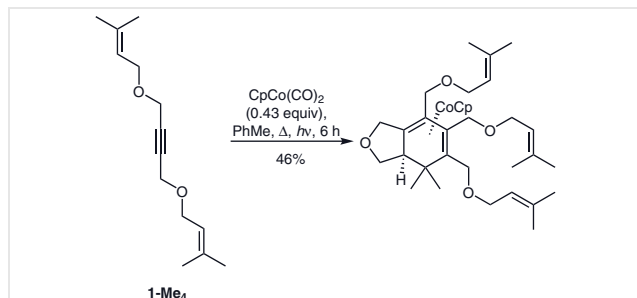


**Scheme 3** Cycloisomerization of **1-Me<sub>2</sub>** featuring  $\beta$ -hydride elimination of only the squared hydrogen in the cobaltacycloheptene intermediate

selectivity,  $\beta$ -hydride elimination engaging exclusively the more hindered side.<sup>1</sup>

Gratifyingly, the experimental results were reproduced computationally (Figure 10). Thus, both *cis* (blue) and *trans* (green) cobaltacycloheptene intermediates **IN2Me<sub>2</sub>** show energetically advantaged  $\beta$ -hydride transfer trajectories involving the more hindered side, with **IN2Me<sub>2</sub>-T-CIS** necessitating a ring flip to **IN2Me<sub>2</sub>-T-CIS-2** before proceeding further. A possible origin of this preference may be the longer (and hence weaker) Co-CMe<sub>2</sub> bond relative to its Co-CH<sub>2</sub> counterpart in **IN2Me<sub>2</sub>** (**IN2Me<sub>2</sub>-T-CIS-2**:  $2.01$  versus  $1.97 \text{ \AA}$ ; **IN2Me<sub>2</sub>-T-TRANS**:  $2.02$  versus  $1.97 \text{ \AA}$ ), although these differences are small. Consideration of the dihedral angle in the participant Co-C-C-H fragment of the various isomers of **IN2** and **TS3**, optimally  $0^\circ$ ,<sup>4e,k,11</sup> gives conflicting numbers. For **IN2Me<sub>2</sub>-T-CIS-2**:  $46^\circ$  (dimethyl side) versus  $50^\circ$ , for **IN2Me<sub>2</sub>-T-TRANS**:  $47^\circ$  versus  $38^\circ$ . The corresponding Co-H distances are  $2.84 \text{ \AA}$  (dimethyl side) versus  $2.98 \text{ \AA}$  and  $3.02 \text{ \AA}$  versus  $2.91 \text{ \AA}$ . Better consonance with the energetics of Figure 10 is found for the dihedral angles in the transition states: **TS3AME<sub>2</sub>-CIS**  $3^\circ$  versus **TS3BMe<sub>2</sub>-CIS**  $4^\circ$ , and **TS3AME<sub>2</sub>-TRANS**  $1^\circ$  versus **TS3BMe<sub>2</sub>-TRANS**  $2^\circ$ , but again the variances are minor. The preceding analyses notwithstanding, their conclusions are highly tentative, as they do not take into consideration the changes in the remaining molecular frame when comparing structures.

Turning to the unobserved exocyclic counterpart of the above  $\beta$ -hydride eliminations involving the hydrogens of one of the methyl groups of **IN2Me<sub>2</sub>** and leading to a skipped diene topology, calculations reveal relatively higher



**Scheme 2** Experimentally observed [2+2+2] co-cycloaddition of **1-Me<sub>4</sub>**

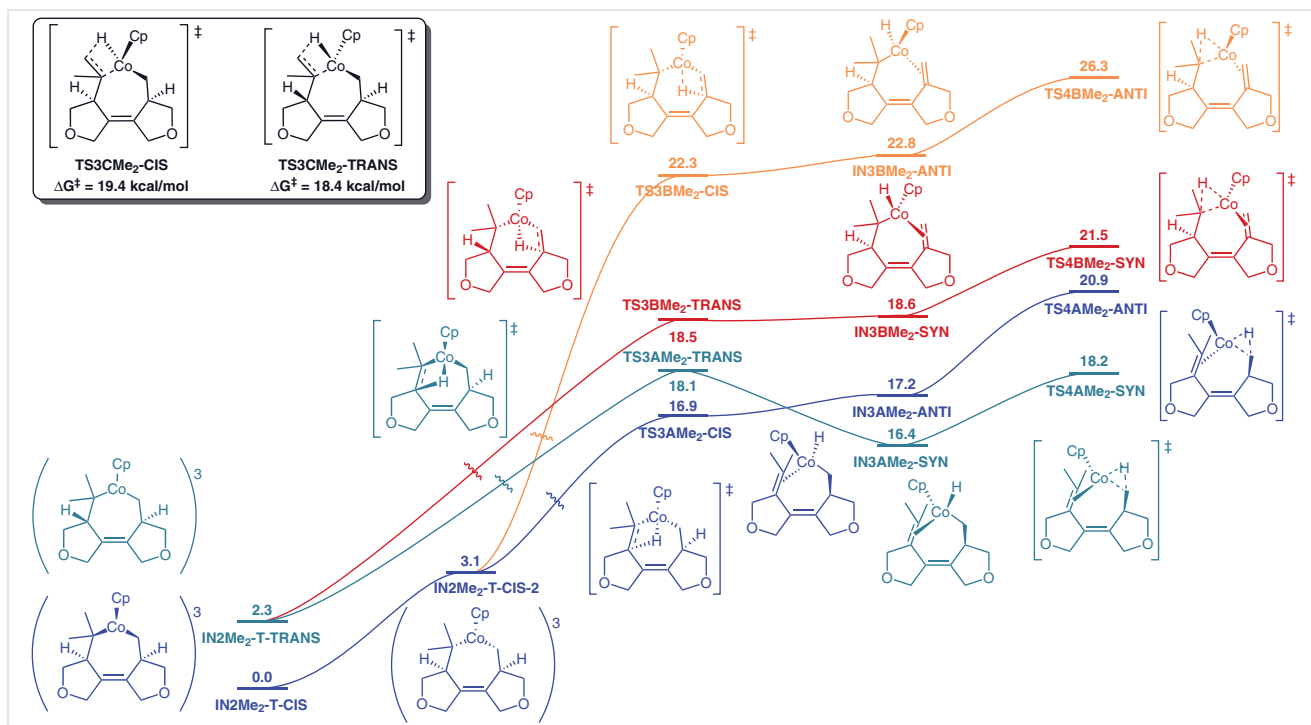
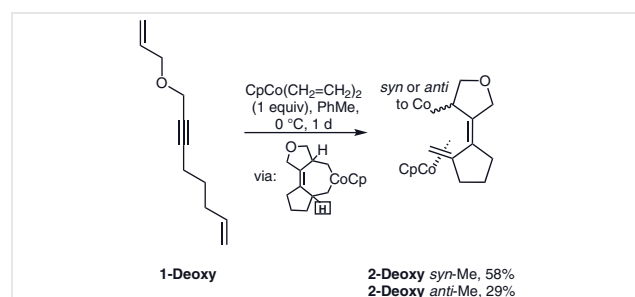


Figure 10 Computational assessment of the  $\beta$ -hydride transfer steps in the cycloisomerization of **1-Me<sub>2</sub>**

barriers (**TS3CMe<sub>2</sub>-CIS**: 19.4 kcal mol<sup>-1</sup> from **IN2Me<sub>2</sub>-T-CIS** and **TS3CMe<sub>2</sub>-TRANS**: 18.4 kcal mol<sup>-1</sup> from **IN2Me<sub>2</sub>-T-TRANS**) (Figure 10) than those of the favored transition states **TS3AME<sub>2</sub>-CIS** and **-TRANS** ( $\Delta G^\ddagger = 13.8$  kcal mol<sup>-1</sup> from **IN2Me<sub>2</sub>-T-CIS-2** and 15.8 kcal mol<sup>-1</sup> from **IN2Me<sub>2</sub>-T-TRANS**, respectively).

Next to be examined was the regioselectivity observed in the cycloisomerization of **1-Deoxy**, which stops at the stage of the deoxy analogue of **2**, engendering **2-Deoxy syn** and *anti* (with respect to the positioning of the methyl substituent and CpCo, ratio 2:1), in turn derived from the corresponding *trans*- and *cis*-cobaltacycloheptene isomers, and exhibits  $\beta$ -hydride elimination exclusively from the non-oxygen containing ring (Scheme 4). Again, computations reproduce this preference (Figure 11), regardless of the stereochemistry of **IN2Deoxy** (cf. the analogous trajectory for **IN2** in Figure 4). Accordingly, starting from **IN2Deoxy-TRANS**, the favored transition state **TS3ADeoxy** that leads to the observed regiochemistry has an activation barrier of 14.3 kcal mol<sup>-1</sup>, while its disfavored counterpart **TS3BDeoxy** is more energetic (15.9 kcal mol<sup>-1</sup>). The reason is plausibly of electronic nature (*vide supra*): the H<sub>2</sub>COCH<sub>2</sub> linker is a much poorer electron donor than its (CH<sub>2</sub>)<sub>3</sub> counterpart and, therefore, cannot as effectively stabilize the partial positive charge that develops on the  $\beta$ -carbon in the transition state.<sup>12</sup> **IN2Deoxy-CIS** (isoenergetic with its *trans* isomer) follows a very similar trail.

A last experimental finding that was addressed computationally was the isomerization of the cyclohexane-fused enyne **1Cy** (Scheme 5). Here, while the furanyl linkage showed the anticipated preference, if incomplete, for the *trans* arrangement, the fusion stereochemistry of the additionally constructed octahydroindene portion emerged exclusively *cis*. In other words, only two of the four possible diastereomers are formed. *In silico* inspection of all potential pathways explains why energetically. The overall most likely reaction trail is depicted in Figure 12 in blue. We start with diastereomer **S-RCCy** (energy zero), so-labelled because it bears the relative *S*-configuration of the cyclohexenyl substituent, while the allylic unit is bound to CpCo in



Scheme 4 Cycloisomerization of **1-Deoxy** featuring  $\beta$ -hydride elimination of only the squared hydrogen in the cobaltacycloheptene intermediate

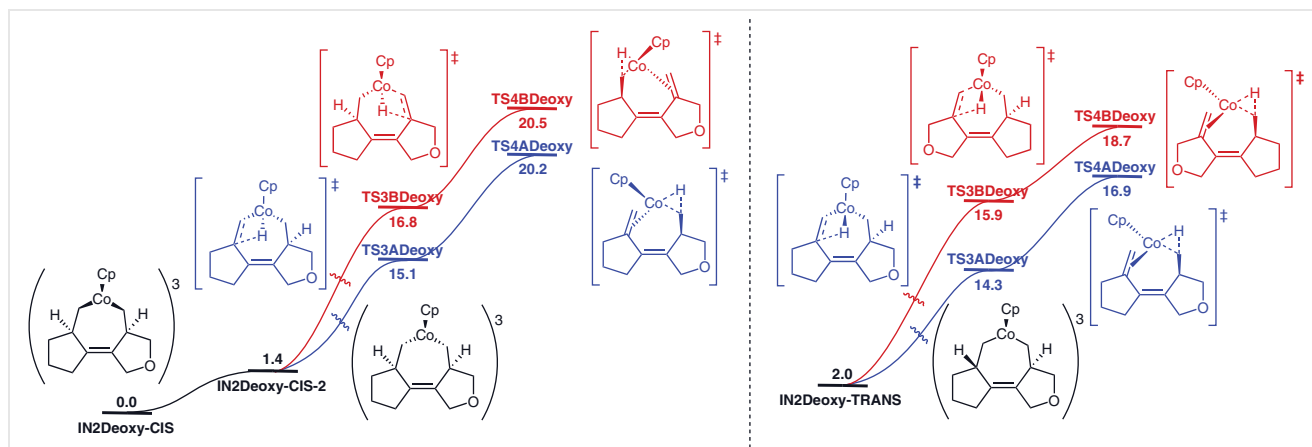
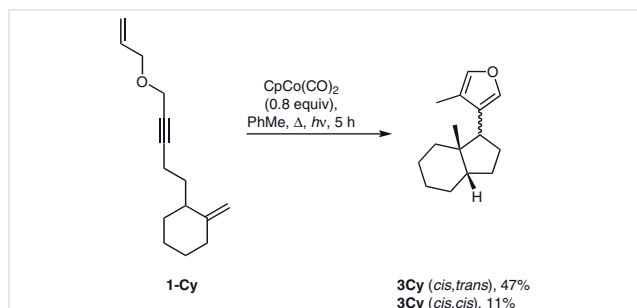


Figure 11 Computed  $\beta$ -hydride elimination of the *cis* and *trans* IN2Deoxy isomers

the favorable *syn*-H form (see Figure 1). This species passes through the overall rate-determining **S-TS1Cy** with a barrier of 19.8 kcal mol<sup>-1</sup> to arrive at **S-IN1Cy-T**, downhill from **S-RCCy** by 7 kcal mol<sup>-1</sup>.



Scheme 5 Conversion of **1-Cy** into two isomers of **3-Cy**

At this stage there are four possible ways by which the dangling methylenecyclohexane can dock the cobaltacyclopentene frame in **S-IN1Cy**: either *syn* or *anti* to the tertiary hydrofuran hydrogen, featuring for each the options of placing the more substituted (hindered) side of the double bond either *endo* or *exo*. As already gleaned from an inspection of simple models,<sup>1</sup> the *endo* variants were too hindered to be computationally tractable, leaving the sequences shown in Figure 12. The lower energy option proceeds via the product-determining **S-TS2Cy-A** ('*syn-exo*'), with a barrier of 14.1 kcal mol<sup>-1</sup> (from **S-IN1Cy-T**) to eventually render **3Cy** (*cis,cis*), one of the experimental products. The alternative (red) route requires 24.1 kcal mol<sup>-1</sup> to travel across **S-TS2Cy-B** ('*syn-exo*'), and would end in the unobserved **3Cy** (*trans,trans*).

Turning to the almost isoenergetic (+0.2 kcal mol<sup>-1</sup>) diastereomer **R-RCCy** (Figure 13), the overall rate-determining activation hill (19.9 kcal mol<sup>-1</sup>) is essentially the same as that for the *S* form and assembles the relatively more stable **R-IN1Cy-T** (−8.3 kcal mol<sup>-1</sup>). From here, the lower ener-

gy pathway (blue) via **R-TS2Cy-A** (9.4 kcal mol<sup>-1</sup>; '*anti-exo*') constructs the other experimentally isolated product **3Cy** (*cis,trans*). The unfavored alternative route (red) **R-TS2Cy-B** (12.7 kcal mol<sup>-1</sup>; '*syn-exo*') would lead to **3Cy** (*trans,cis*) and could not be computed beyond **R-IN2Cy-B**. Again, the *endo* variants were too hindered to be computationally tractable. As in the discussion of the results in Figures 2 and 3, a contributing factor to the relative stability of transition states **S-** and **R-TS2Cy-A** may be the near parallel (optimal)<sup>7,11a</sup> geometries of the inserting alkene moieties and their target Co–C $\alpha$  bonds (4 and 5°, respectively), compared to their higher-energy relatives (12 and 13°).

To conclude, DFT appraisals have allowed the energetically and structurally detailed determination of the mechanistic aspects of the title reactions. For the prototype conversion of 1,4-bis(2-propenyloxy)but-2-yne (**1**), the two tracks ending in *trans*-tetrahydrofuranfuran **3** and its *cis*-isomer are very close in energy (Figures 1, 4 and 6). Their key features are preferential complexation of the double bond in enyne complex **RC** in the *syn*-H configuration, followed by a rate-determining early oxidative coupling step via **TS1**, and stereoselective second double bond incorporation via **TS2-EXO** and **-ENDO** to generate the two cobalta-4-cycloheptenes **IN2-CIS** and **-TRANS**, whose stereochemistry is the origin of that in the final products. These species enter into ready  $\beta$ -hydride elimination–reductive elimination sequences to construct the relatively low energy CpCo- $\eta^4$ -dienes **IN4-SYN** (isolated as **2** at 0 °C) and **-ANTI**. The subsequent cascade of hydrogen shifts exhibit **TS6-SYN** and **-ANTI** as rate-determining and with energies commensurate with the conversion of **2** into **3** at 80–100 °C. Overall,  $\Delta G_1 \rightarrow 3 = 50.8$  kcal mol<sup>-1</sup>. The experimental observations of chemo-, regio-, and stereoselectivity with modified versions of **1** were also nicely corroborated by computation. Accordingly, **1-Me<sub>4</sub>** (Scheme 2 and Figure 9) was indeed too hindered to be competitive with intermolecular [2+2+2] cycloaddition. The regioselective transformation of **1-Me<sub>2</sub>** (Scheme 3 and



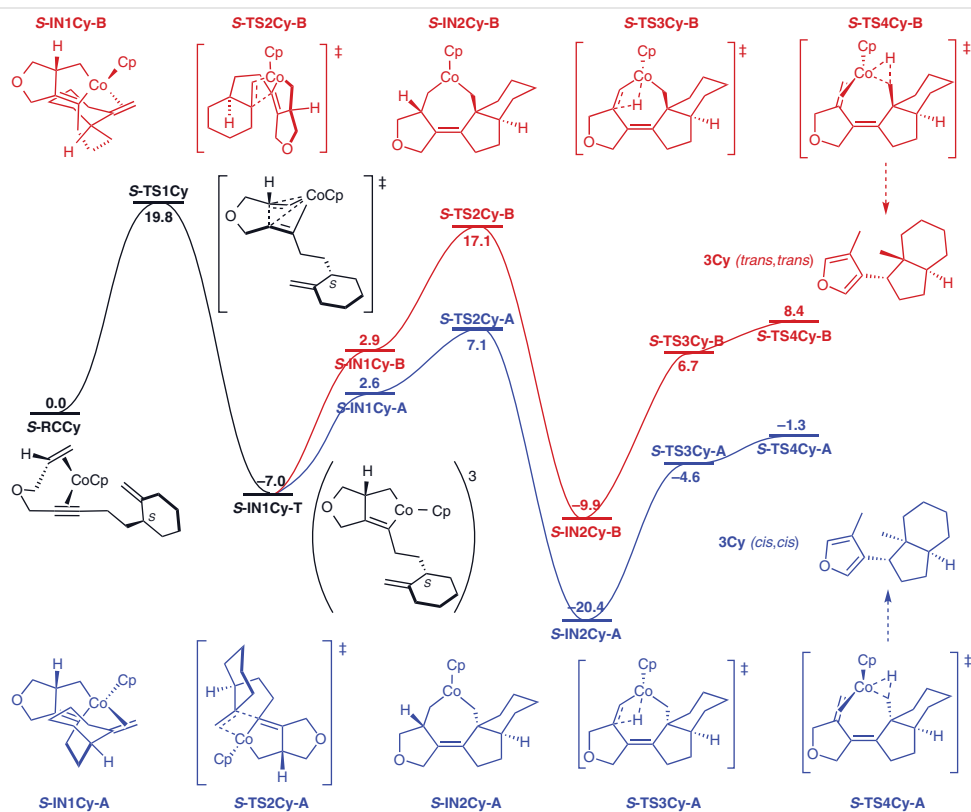


**Figure 12** Abbreviated computed trajectory of the cyclization of **1Cy** to give *cis,cis* **3Cy** (blue) and its unobserved *trans,trans* (red) isomer

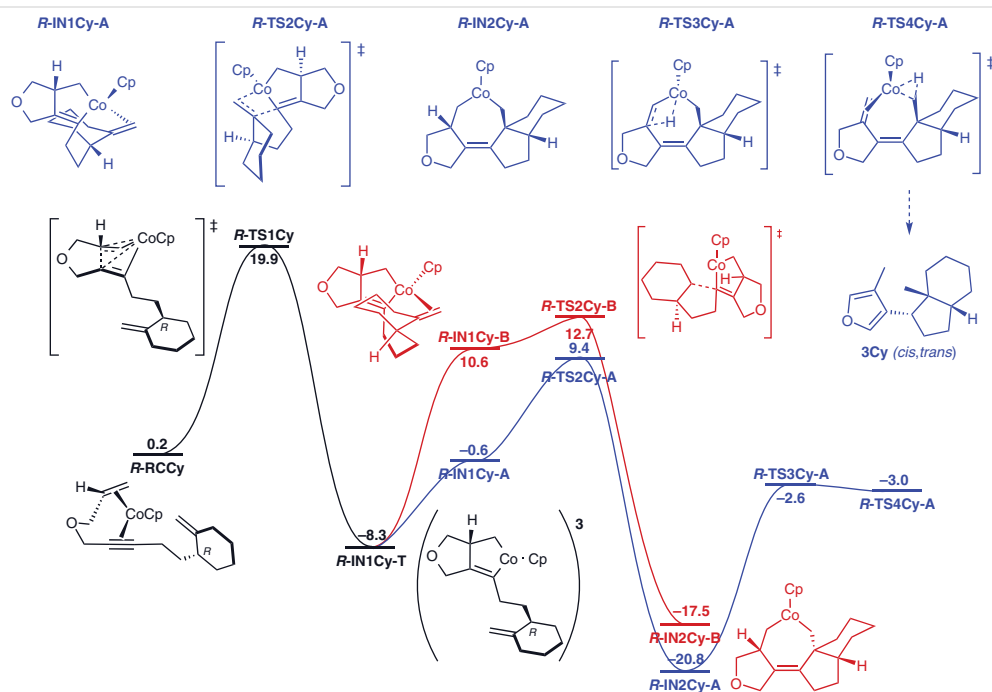


**Figure 13** Abbreviated computed trajectory of the cyclization of **1Cy** to give *cis,trans* **3Cy** (blue). The red sequence (to the *trans,cis* isomer) could not be extended beyond **R-IN2Cy-B**.

Figure 10) could be traced back to bond strength and charge considerations of the  $\beta$ -hydride eliminations emanating from **IN2Me<sub>2</sub>**, the more substituted side winning out. Similarly, **1-Deoxy**, the cyclization of which stops at the stage of complex **2-Deoxy** (Scheme 4), prefers  $\beta$ -hydride eliminations away from the oxygen-containing ring due to the electron-withdrawing nature of the proximal heteroatom (Figure 11). Finally, the added stereochemical complexity introduced by the presence of a stereocenter in **1Cy** into the cyclization manifold was scrutinized, providing a clear validation for the selectivity of its cycloisomerization (Scheme 5). Specifically, of the eight possible **IN1Cy** intermediates and subsequent transition states **TS2Cy**, four were too sterically compromised to be tractable by computation. Of the remaining four, two were energetically clearly favored and led to the two observed isomers (Figures 12 and 13).

## Conflict of Interest

The authors declare no conflict of interest.

## Funding Information

This work benefited from pecuniary support by the University of California at Berkeley (K.P.C.V.). We are grateful to the National Science Foundation (CHF-1764328 to K.N.H.) for financial support. Calculations were performed on the Hoffman2 cluster at the University of California, Los Angeles, and the Extreme Science and Engineering Discovery Environment (XSEDE), which is supported by the National Science Foundation (OCI-1053575).

## Supporting Information

Supporting information for this article is available online at <https://doi.org/10.1055/a-1645-2632>.

## References

- (1) Chang, C.-A.; Gürtzgen, S.; Johnson, E. P.; Vollhardt, K. P. C. *Synthesis* **2020**, 52, 399.
- (2) For some recent reviews of related isomerizations, see: (a) Liu, X.; Li, B.; Liu, Q. *Synthesis* **2019**, 51, 1293. (b) Ai, W.; Zhong, R.; Liu, X.; Liu, Q. *Chem. Rev.* **2019**, 119, 2876. (c) Hirano, M. *ACS Catal.* **2019**, 9, 1408. (d) Pellissier, H. *Coord. Chem. Rev.* **2018**, 360, 122. (e) Hu, Y.; Bai, M.; Yang, Y.; Zhou, Q. *Org. Chem. Front.* **2017**, 4, 2256. (f) Chen, W.-W.; Xu, M.-H. *Org. Biomol. Chem.* **2017**, 15, 1029. (g) Röse, P.; Hilt, G. *Synthesis* **2016**, 48, 463. (h) Stathakis, C. I.; Gkizis, P. L.; Zografos, A. L. *Nat. Prod. Rep.* **2016**, 33, 1093. (i) Gandeepan, P.; Cheng, C.-H. *Acc. Chem. Res.* **2015**, 48, 1194. (j) Micalizio, G. C.; Hale, S. B. *Acc. Chem. Res.* **2015**, 48, 663.
- (3) For a topical review, see: (a) Domínguez, G.; Pérez-Castells, J. *Chem. Eur. J.* **2016**, 22, 6720. For examples of pertinent intramolecular dienyne cycloisomerizations, see ref. 1 and: (b) Suleymanov, A. A.; Vasilyev, D. V.; Novikov, V. V.; Nelyubina, Y. V.; Perekalin, D. S. *Beilstein J. Org. Chem.* **2017**, 13, 639; and references cited therein. (c) Lanzi, M.; Santacrose, V.; Balestri, D.; Marchiò, L.; Bigi, F.; Maggi, R.; Malacria, M.; Maestri, G. *Angew. Chem. Int. Ed.* **2019**, 58, 6703; and references cited therein.
- (4) For an excellent review, see: (a) Roglans, A.; Pla-Quintana, A.; Solà, M. *Chem. Rev.* **2021**, 121, 1894. For a collection of specific examples, see: (b) Delorme, M.; Punter, A.; Oliveira, R.; Aubert, C.; Carissan, Y.; Parrain, J.-L.; Amatore, M.; Nava, P.; Commeiras, L. *Dalton Trans.* **2019**, 48, 15767. (c) Anderson, E. A.; Paton, R. S. *Chimia* **2018**, 72, 614. (d) Cassú, D.; Parella, T.; Solà, M.; Pla-Quintana, A.; Roglans, A. *Chem. Eur. J.* **2017**, 23, 14889. (e) Kiyota, S.; In, S.; Komine, N.; Hirano, M. *Chem. Lett.* **2017**, 46, 1040. (f) Yang, T.; Ehara, M. *J. Org. Chem.* **2017**, 82, 2150. (g) Mekareeya, A.; Walker, P. R.; Couce-Rios, A.; Campbell, C. D.; Steven, A.; Paton, R.; Anderson, E. A. *J. Am. Chem. Soc.* **2017**, 139, 10104. (h) Hirano, M.; Ueda, T.; Komine, N.; Komiya, S.; Nakamura, S.; Deguchi, H.; Kawauchi, S. *J. Organomet. Chem.* **2015**, 797, 174. (i) Haraburda, E.; Torres, O.; Parella, T.; Solà, M.; Pla-Quintana, A. *Chem. Eur. J.* **2014**, 20, 5034. (j) Liu, T.; Han, L.; Han, S.; Bi, S. *Organometallics* **2014**, 34, 280. (k) Hong, X.; Liu, P.; Houk, K. N. *J. Am. Chem. Soc.* **2013**, 135, 1456. (l) Dachs, A.; Pla-Quintana, A.; Parella, T.; Solà, M.; Roglans, A. *Chem. Eur. J.* **2011**, 17, 14493. (m) Varela, J. A.; Saá, C. J. *Organomet. Chem.* **2009**, 694, 143. (n) Clavier, H.; Correa, A.; Escudero-Adán, E. C.; Benet-Buchholz, J.; Cavallo, L.; Nolan, S. P. *Chem. Eur. J.* **2009**, 15, 10244. (o) Montero-Campillo, M. M.; Rodríguez-Otero, J.; Cabaleiro-Lago, E. *J. Phys. Chem. A* **2008**, 112, 2423.
- (5) For our DFT appraisals with pertinent CpCo systems, see: (a) Leboeuf, D.; Iannazzo, L.; Geny, A.; Malacria, M.; Vollhardt, K. P. C.; Aubert, C.; Gandon, V. *Chem. Eur. J.* **2010**, 16, 8904. (b) Aubert, C.; Gandon, V.; Geny, A.; Heckrodt, T. J.; Malacria, M.; Paredes, E.; Vollhardt, K. P. C. *Chem. Eur. J.* **2007**, 13, 7466. (c) Geny, A.; Leboeuf, D.; Rouquié, G.; Vollhardt, K. P. C.; Malacria, M.; Gandon, V.; Aubert, C. *Chem. Eur. J.* **2007**, 13, 5408. (d) Agenes, N.; Gandon, V.; Vollhardt, K. P. C.; Malacria, M.; Aubert, C. *J. Am. Chem. Soc.* **2007**, 129, 8860. (e) Gandon, V.; Agenes, N.; Vollhardt, K. P. C.; Malacria, M.; Aubert, C. *J. Am. Chem. Soc.* **2006**, 128, 8509.
- (6) Hong, P.; Yamamoto, Y.; Yamazaki, H. *J. Organomet. Chem.* **1982**, 232, 71.
- (7) For a review, see: Espinet, P.; Albéniz, A. C. In *Fundamentals of Molecular Catalysis*; Kurosawa, H.; Yamamoto, A., Ed.; Elsevier: Amsterdam, **2003**, 293.
- (8) The cycloheptene frame is conformationally very flexible, see: (a) Leong, M. K.; Mastryukov, V. S.; Boggs, J. E. *J. Mol. Struct.* **1998**, 445, 149. (b) Borgen, G. *Acta Chem. Scand., Ser. B* **1974**, 28, 135. (c) St. Jacques, M.; Vaziri, C. *Can. J. Chem.* **1971**, 49, 1256. (d) Neto, N.; Di Lauro, C.; Califano, S. *Spectrochim. Acta, Part A* **1970**, 26, 1489. (e) For the first postulation of such a cobalt-cycloheptene ring flip, see: Wakatsuki, Y.; Aoki, K.; Yamazaki, H. *J. Am. Chem. Soc.* **1979**, 101, 1123. (f) See also: Scozzafava, M.; Stolzenberg, A. M. *Organometallics* **1988**, 7, 1073.
- (9) (a) Cammack, J. K.; Jalisatgi, S.; Matzger, A. J.; Negrón, A.; Vollhardt, K. P. C. *J. Org. Chem.* **1996**, 61, 4798. (b) King, J. A. Jr.; Vollhardt, K. P. C. *J. Organomet. Chem.* **1993**, 460, 91.
- (10) For a tabulation of van der Waals radii, see: Alvarez, S. *Dalton Trans.* **2013**, 42, 8617.
- (11) For selected pertinent discussions of steric and electronic effects on  $\beta$ -hydride eliminations, see: (a) Chen, Z.-M.; Liu, J.; Guo, J.-Y.; Loch, M.; DeLuca, R. J.; Sigman, M. S. *Chem. Sci.* **2019**, 10, 7246; and references cited therein. (b) Giri, R.; Shekhar, K. C. *J. Org. Chem.* **2018**, 83, 3013. (c) Jana, R.; Pathak, T. P.; Sigman, M. S. *Chem. Rev.* **2011**, 111, 1417. (d) Gómez-Gallego, M.; Sierra, M. A. *Chem. Rev.* **2011**, 111, 4857. (e) Piers, W. E.; Collins, S. In

*Comprehensive Organometallic Chemistry III, Vol. 1*; Mingos, D. M. P.; Crabtree, R. H., Ed.; Elsevier: Amsterdam, **2007**, 141. (f) Lu, X. *Top. Catal.* **2005**, *35*, 73. (g) Sen, A.; Kang, M. In *Late Transition Metal Polymerization Catalysis*; Rieger, B.; Saunders Baugh, L.; Kacker, S.; Striegler, S., Ed.; Wiley-VCH: Weinheim, **2003**, 307. (h) Trost, B. M.; Romero, D. L.; Rise, F. *J. Am. Chem. Soc.* **1994**, *116*, 4268. (i) Trost, B. M.; Tanoury, G. J.; Lautens, M.; Chan, C.; MacPherson, D. T. *J. Am. Chem. Soc.* **1994**, *116*, 4255.

(j) Trost, B. M.; Lautens, M.; Chan, C.; Jebaratnam, D. J.; Mueller, T. *J. Am. Chem. Soc.* **1991**, *113*, 636. (k) Trost, B. M.; Lee, D. C.; Rise, F. *Tetrahedron Lett.* **1989**, *30*, 651.

- (12) (a) For a seminal report, see: Doherty, N. M.; Bercaw, J. E. *J. Am. Chem. Soc.* **1985**, *107*, 2670; and citing references (b) For a recent treatment, see: Wheeler, J. I.; Carlsen, R.; Ess, D. H. *Dalton Trans.* **2020**, *49*, 7747.